Technical Report

Extraction of Macro-molecule Images in Cryo-EM Micrographs

PS Umesh Adiga[1], Ravi Malladi[2], Robert M Glaeser[3]

Abstract

Advances in Electron Microscopy and single-particle reconstruction have led to results at increasingly high resolutions. This has opened up the possibility of complete automation of single particle reconstruction. Main bottleneck in automation of single particle reconstruction is manual selection of particles in the micrograph. This paper describes a simple but efficient approach for segmentation of particle projections in the micrographs obtained using cryo-electron microscope. Changing the shape of objects to facilitate segmentation from the cluster and reconstructing its actual shape after isolation is successfully attempted. Both low-level and high-level processing techniques are used and the whole process is made automatic. Over 90% success in automatic particle picking is achieved. Several areas for improvement and future research directions are discussed.

Keywords: micrograph, particle, projection, macro-molecule, segmentation

[1] Author for correspondence, Bio-Imaging Group, MS84-171, LBNL, 1, Cyclotron Road, Berkeley, CA94705, Email: upadiga@lbl.gov

[2] Staff Scientist, Division of Mathematics and Computer Science, LBNL, 1, Cyclotron Road, Berkeley CA94705, Email: malladi@math.lbl.gov

[3] Principal Scientist and Professor of Structural Biology, Room 365, Donner, UC Berkeley, Berkeley CA94720, Email: RMGlaeser@lbl.gov

This work was supported by the Director, Office of Science, of the U.S. Department of Energy under Contract No. 619701

I. Introduction

Electron or cryo-Electron Microscopy (cryoEM) has matured into a powerful and diverse collection of methods that facilitate visualization of macromolecular structure and dynamics of an extraordinarily broad range of macromolecules and macromolecular assemblies. Electron micrographs of vitrified specimens are recorded at very low electron dose to minimize radiation damage, resulting in low image contrast [1]. This requires image processing of micrographs of millions of molecules to increase the signal-to-noise ratio.

Number of macro-molecule images required for a volumetric reconstruction increases dramatically with the resolution of the micrograph. When images of currently available quality are used, it is believed that at least one million images are required to reconstruct a macro-molecule with “atomic” resolution. For processing the micrograph images, particles from each micrograph are selected either manually, using interactive graphics software or by computer aided semi-automatic methods. This is a very labor intensive, fatiguing job that is prone to human error. Thus complete automation of particle selection is necessary to prevent this stage from becoming a serious bottle neck in achieving reproducible structure/shape of a protein molecule.

Several approaches to automatic shape extraction of a macro-molecule have been proposed and have met with varying degree of success. These approaches include methods that make use of various forms template matching, local comparison of intensity values, edge detection, quantitative measures of the local image texture/statistics, etc. Success in cryoEM invariably depends on techniques that combat the inherently low image contrast, as well as reducing deleterious effects such as specimen drift and electron beam-induced charging. These problems occur during the recording of image and all too often degrade image quality. High-resolution studies in particular put stringent demands on instrument stability and sample preservation.

Faster computers and efficient data storage allow ever greater amounts of data to be analyzed. This is essential for pushing the resolution limits in single particle analysis, which requires very large numbers of individual particles to be processed, aligned, and averaged. Programs for processing high-resolution images of two-dimensional (2D)

protein crystals are now well established [4]. Programs for processing of tubular crystals with helical symmetry at high resolution are well under way [5] and similar programs are being developed for single particles (e.g. [6]). As image processing methods for correcting electron optical effects such as defocus, image astigmatism and beam tilt are developed and refined, it should soon become possible to achieve resolutions that reveal secondary structure and even near-atomic detail in unsymmetrical particles as well. In interactive particle selection method, a digitized micrograph is displayed on the screen of workstation for selection of suitable particles. Considering several problems associated with display of large images to interactively select particles, most of the software tools make a trade-off between size reduction of the image and amount of scrolling needed to do on Graphical User Interface (GUI) to visualize complete image.

Interactive selection is subjective and hence may not be reproducible. Considering the large number of particles to be extracted, interactive selection is not a feasible option. Van Heel [13], Frank and Wagenknecht [16], Andrews et al [18]; have developed early automation techniques to reduce the interaction in particle selection. These attempts have met with partial success due to non-availability of powerful computers at that time. Schemes based on thresholding, component labeling, feature computation and symbolic manipulation of the result was proposed by Harauz and Fong-Lochocsky [19]. Lata et al [20] have proposed particle extraction based on texture feature of the components obtained by peak search of the Gaussian smoothed micrograph. Though these methods showed encouraging results, still many false positives get through and a manual editing of the data is required as a final step. For further details, we suggest a review article by Nicholson and Glaeser [21] for detailed review of various pattern recognition techniques that could be applied to extract macromolecules from cryoEM micrographs.

In spite of advancement in pattern recognition and image processing, there is a large gap between what has been achieved in applied image processing and single particle extraction from micrographs. In this article, we present a novel methodology of integrating several filters that forces the object shape to suit isolation of touching particles or enhancement of contrast between particle projection and its background. After extraction of individual particle signatures, its actual shape is recovered. Our focus is not just extraction of single particles but to segment those single particles which are

located very close to one-another. Results obtained are very encouraging and we plan to develop a comprehensive tool set to automatically extract single particles and construct a 3-D shape.

II. Pre Processing Techniques and Segmentation

Electron microscope images of macromolecules lack clarity and definition in-addition to limited resolution and instrument electronic noise. Before attempting to extract objects (projections of particles) from the image, it is important to suppress extraneous information not related to the object. It is difficult to control the noise sources and hence it is prudent to develop intelligent algorithms that may suppress the noise in the image.

1. Re-sampling approach to reduce the fine texture of the background

Figure 1(a), shows an example image of ribosome particles embedded in thin ice. It can be observed that background image has a definitive texture pattern. If we can device a strategy to extract this pattern and subtract it from original image, a residual image with only particle signatures can be obtained. One of the methods that can be effectively used is re-sampling approach or multi-scale approach. Here the image is re-sampled in such a way that the particle signatures shrink to a level that it is not possible to distinguish particle signature from the surrounding texture.

In another approach to image difference method, background patches from different parts of the image are collected. A complete background image is reconstructed by these texture patterns. This background image provides a frequency range of the background texture that can be suppressed in frequency domain analysis. This increases the contrast between particle projections and the rest in the micrograph.

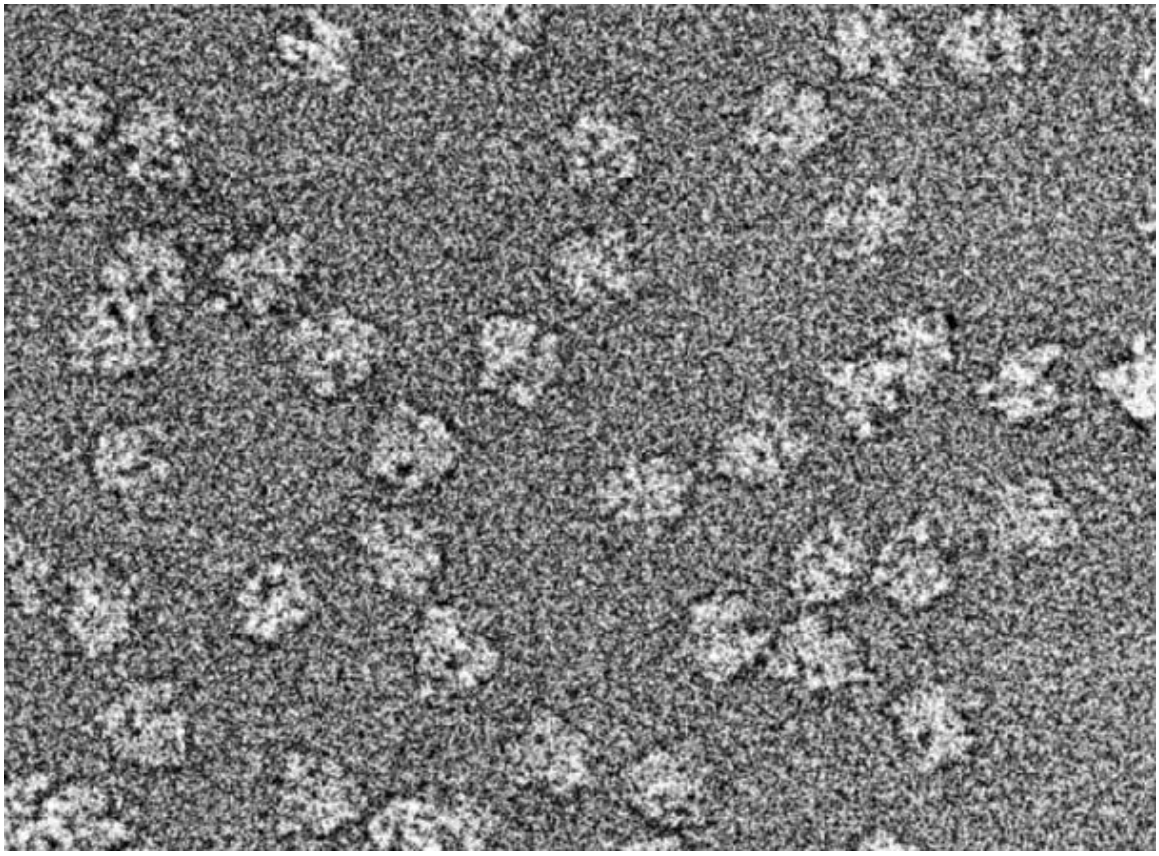

Figure 1: (a) Small part of original micrograph of ribosome particles embedded in ice

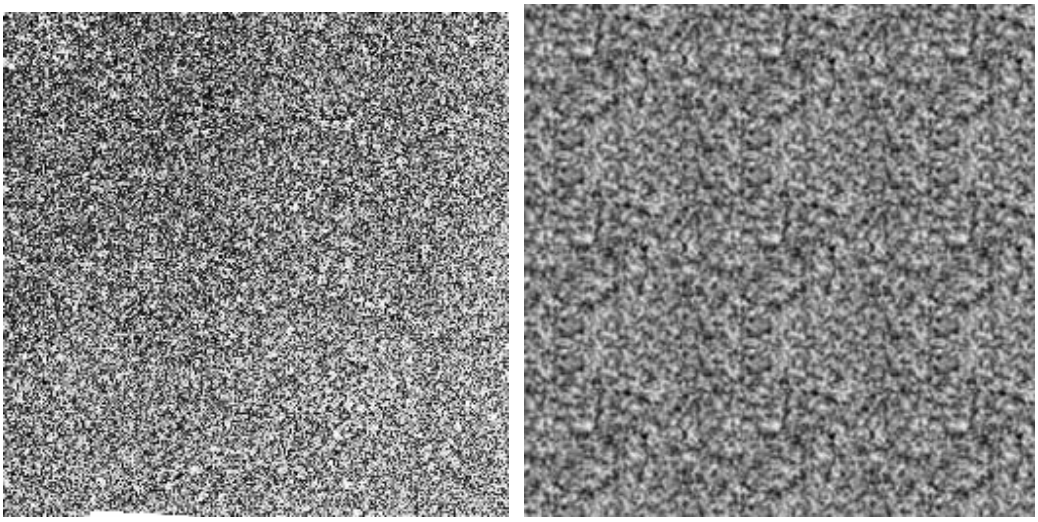

(b) (c)

Figure 1(b): After re-sampling the original 2048 x 2048 image to 256 x 256 image (c) Background image reconstructed from background patches.

Figure 1(b), shows such a re-sampled image. Original image (in Figure 1(a)) is of size 2048 x 2048 but only a part of it is shown here. Original image is sampled to 256 x 256

and shown in figure 1(b). If we add a step of smoothing after first stage of sampling (that is when the image was sampled to 1024 x 1024) and then sampled to 256 x 256, we obtain a better result at distinguishing particles from the background. Figure 2, shows the result of such a process.

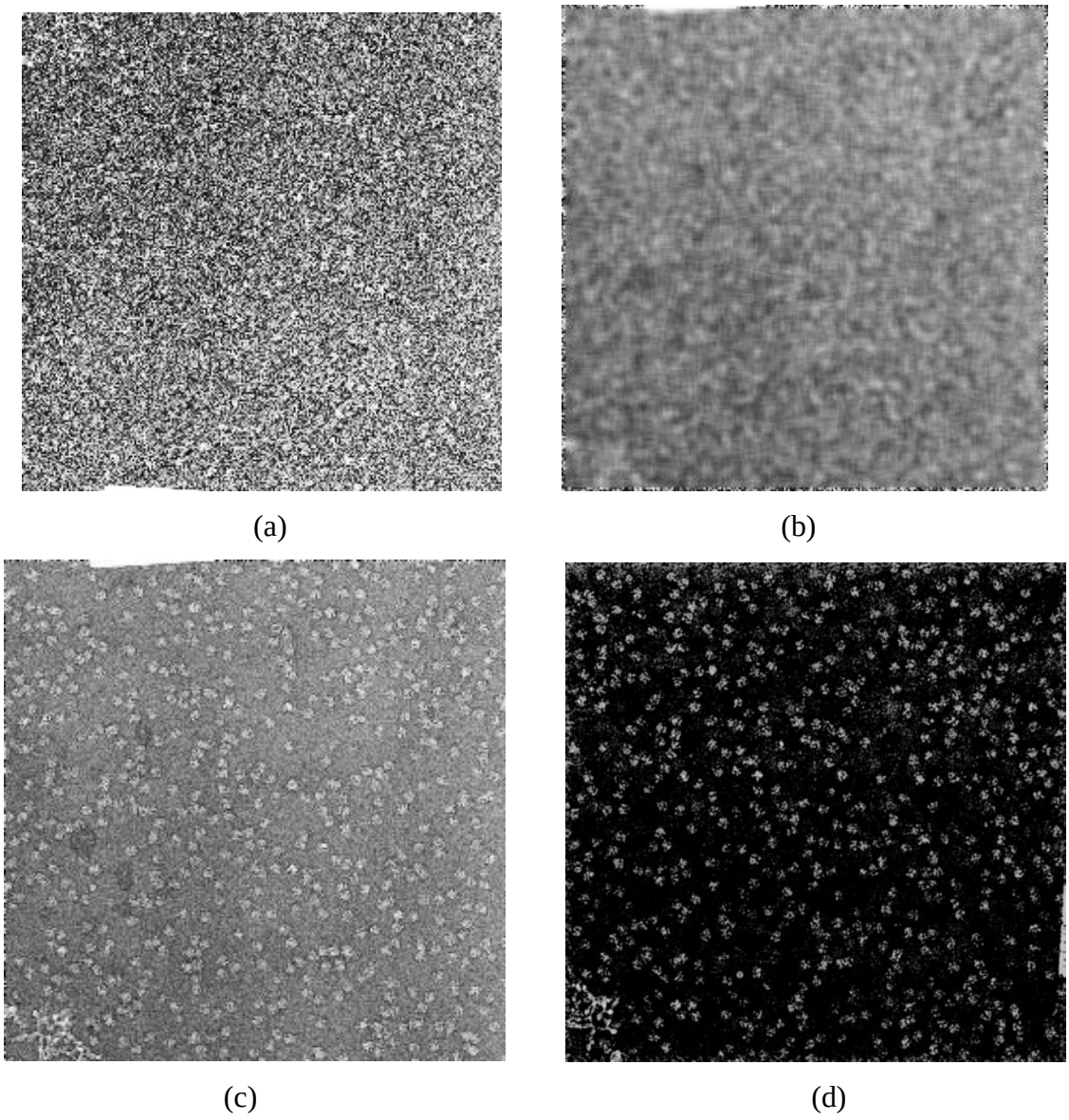

(a) (b)

(c) (d)

Figure 2: (a) Original image sampled to 256x256, (b) Smoothing Figure 2(a) by moving average filter (c) Result of sampling the original image after smoothing by moving average filter, (d) Result of image difference method using interactively reconstructed background.

2. Polynomial Fitting for Reducing Background Illumination Variation

Due to variation in the sample thickness and other factors micrographs show uneven illumination. Such illumination variation can be corrected by least square fitting. By selecting a number of points or samples, a list of brightness values can be acquired. These sample values can then be used to reconstruct the approximate background by performing least-square fitting. Such a background is then subtracted from the original image to reduce the effect of uneven illumination in the image.

Select number of equidistant points from the image such that each sample point is the average brightness of appropriate size neighborhood. A background function is constructed using such sampled values by least-square fitting. $(m,n)^{\text{th}}$ order bivariate polynomial can be written as

$$B(x,y) = a_{mn}x^m y^n + ... + a_{22}x^2y^2 + a_{21}x^2y^1 + a_{12}x^1y^2 + a_{11}xy + a_{10}x + a_{01}y + a_{00}$$

Bivariate polynomial function we have used in our experiment is

$$B(x,y) = a_{22}x^2y^2 + a_{21}x^2y^1 + a_{12}x^1y^2 + a_{11}xy + a_{10}x + a_{01}y + a_{00}$$

Brightness of the sampled points is used to calculate the seven fitted constants or seven coefficients of the second order polynomial by least-squares. Using these coefficients, a complete background image is reconstructed.

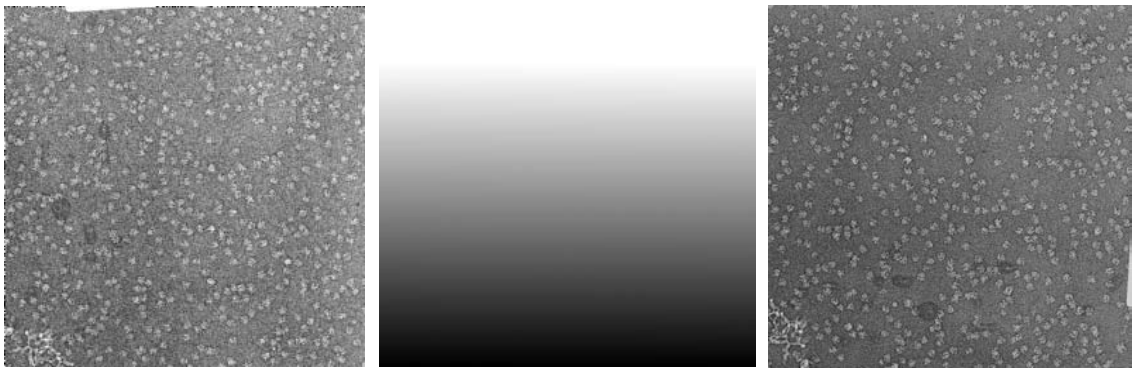

(a) (b) (c)

Figure 3: Smoothed and sampled original image showing illumination variation, (b) Background variation (brightness is scaled 0-255 for better visualization), (c) Background corrected by least-square fitting (only partial image is shown)

This background image more-or-less represents background brightness variation in the original image. Background image is subtracted from the original image. All negative pixel values are clipped to zero. Resulting image is rescaled to occupy complete grey-level spectrum of 0-255.

4. Rank-leveling Approach for Reducing Background Variation

Though least-square fitting works satisfactorily in reducing major variation in the illumination, it is found to leave local variations intact. Such a local variation can be reduced by rank-leveling approach. Rank leveling is a process where grey level of a pixel is replaced by minimum grey level in its neighborhood till the objects in the image disappear. Neighborhood size is selected based on approximate size of the object. If the objects are darker than background, we replace the pixel grey level by the maximum in its neighborhood. Resulting image can be argued as representation of the background image and is subtracted from the original. Figure 5 shows an example of application of rank leveling to micrograph.

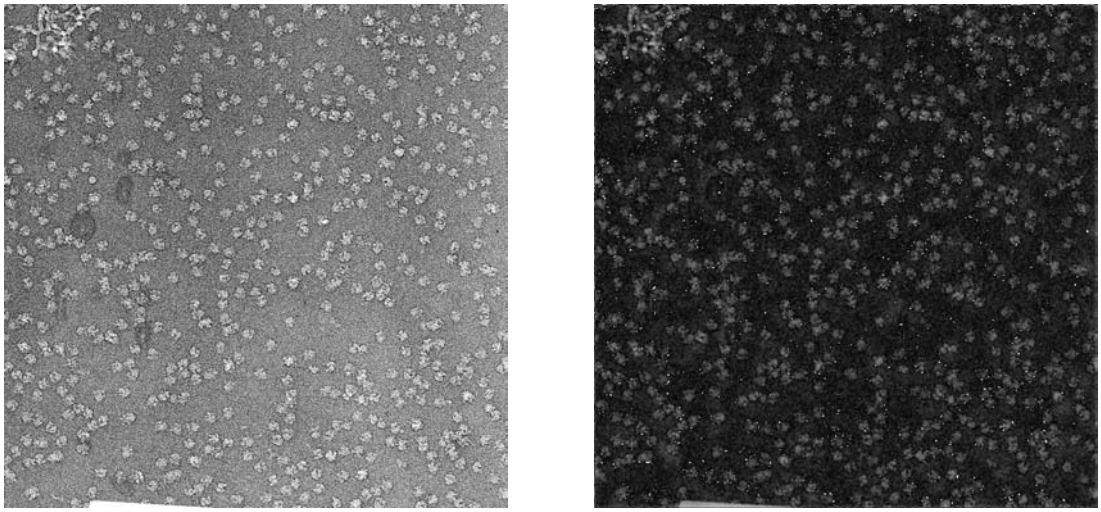

(a) (b)

Figure 5: (a) Original image re-sampled smoothed and re-sampled, (b) After rank leveling to suppress the background

5. Detection and Segmentation of Particle Signature

Each micrograph is pre-processed by above mentioned methods before applying segmentation techniques. In the first stage of background separation, smoothed image is amplitude thresholded at a global mean intensity value $(k\mu)$ where k is a tuning parameter set experimentally and μ is the global mean intensity. All connected components in the foreground are identified by component labeling. In the second stage, the mean grey level μ_i of connected component i is calculated. Connected component i is further thresholded at a unique threshold value ($k_1 \cdot \mu_i$).

Tuning factor k_1 is experimentally set (default k_1 = 0.5). Figure 6, shows the result of thresholding and component labeling a pre-processed micrograph (shown partially).

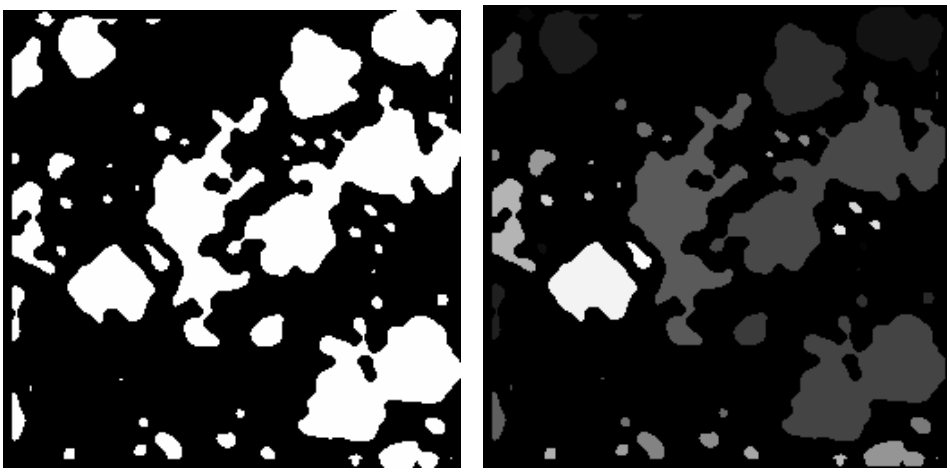

(a) (b)

Figure 6: (a) Thresholded image (b) Component labeled image

Grey scale morphological operation such as 'opening' and 'closing' with an appropriate structuring element is very important to isolate actual particle projections and particle clusters from the rest. A bank of structuring elements with circular effective kernel is designed for morphological operation. Using a suitable structuring element, two-tone image is 'opened'. This eliminates small noisy objects that resulted from thresholding highly textured micrographs. Closing operation using appropriate structuring element with a circular effective kernel removes holes in the foreground/signature of particle projections. It also forces the signature of particle projections to have convex/circular shape that can be better segmented by standard segmentation techniques. Figure 7(a) and Figure 7(b), shows the signatures after morphological filtering that force the signatures to be more convex/circular.

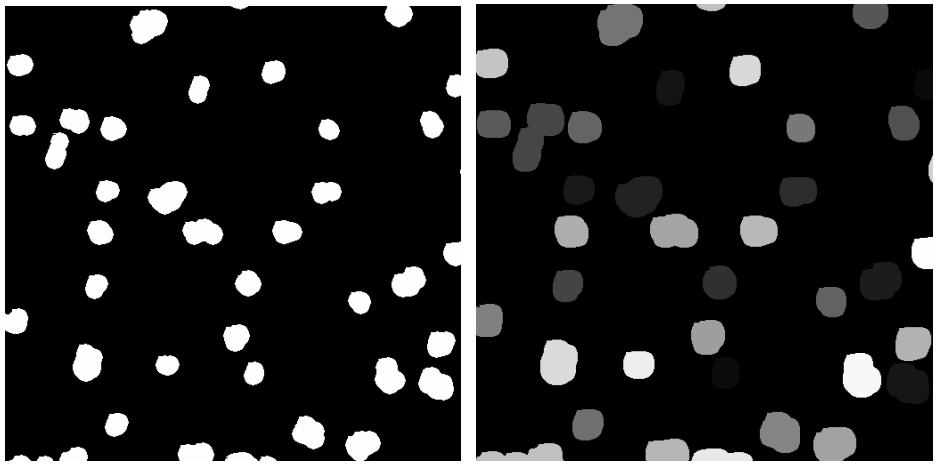

(a) (b)

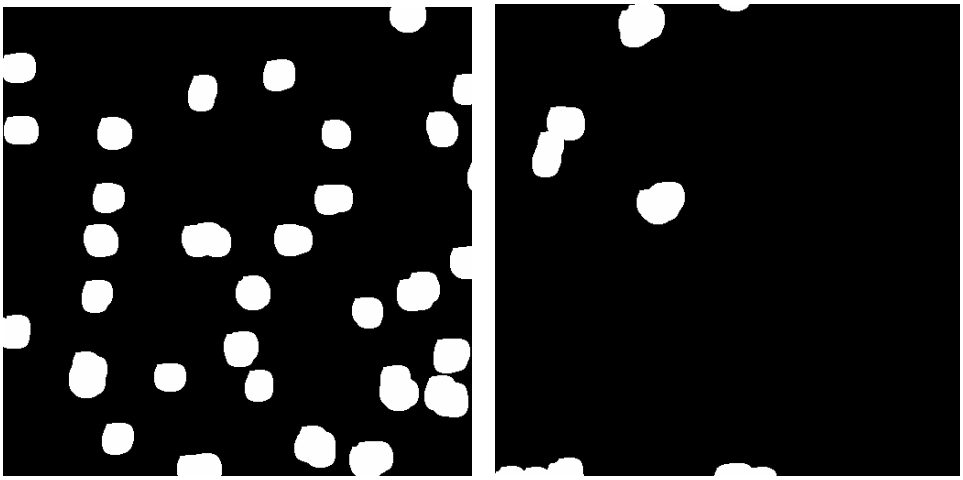

(c) (d)

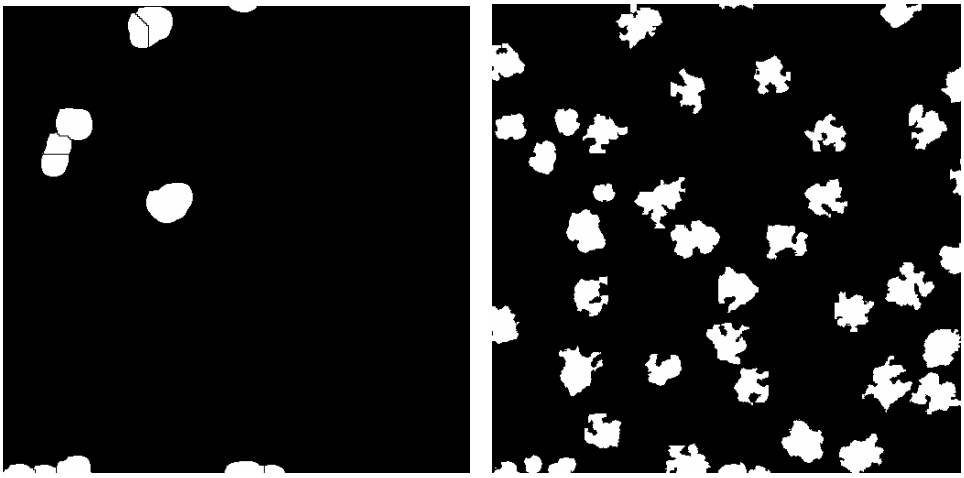

(e) (f)

Figure 7: After morphological opening and closing with a circular structuring element (b) After expanding the signatures by three iterations and labeling (only partial micrograph is shown) (c) Signatures extracted as isolated signatures based on relative features, (d) Signatures flagged of for next stage of segmentation (e) After segmentation by watershed (f) After grey scale shrinking to extract the actual shape of the particle projections (only partial micrograph is shown).

It is necessary to recognize individual or cluster of particles in the segmented image. Isolated particles are recognized based on its relative size and intensity features. Relative size of the object r_v is defined as the ratio of the size of the object to average size of objects in the image. If average size of object i is $\overline{V_i}$, then $r_{v_i} = \dfrac{\overline{V_{i_i}}}{\dfrac{1}{\beta}\cdot\sum_{i=1}^{\beta}\overline{V_i}}$, where β is the number of isolated objects present in the image. Relative intensity of the object r_{I_i} is defined as the ratio of the average intensity of the object pixels to average intensity of foreground pixels in the image. If average intensity of object i is $\overline{I_i}$, then $r_{I_i} = \dfrac{\overline{I_{i_i}}}{\dfrac{1}{N_f}\cdot\sum_{k=1}^{N_f} I_k}$, where N_f is the number of foreground pixels in the image. The relative object size and relative object intensity of each individual object in the image are calculated for all the objects in the image.

Average size is calculated by α-cut filter which excludes α number of extreme size elements in size order list of objects for calculation of average object size $\overline{V_i}$ in the image. All those objects with relative mean object intensity less than 0.3 are considered as artifacts and eliminated (this threshold is set experimentally). Figure 7(c) and Figure 7(d), shows the result of elimination of noisy objects from a thresholded and labeled micrograph (shown partially). One's with relative mean object intensity more than 1.2 are considered as possible clusters and flagged off for further segmentation.

6. Segmentation of Closely Located Particles

This is an important step that defines the success of automation of extraction of single particle images from micrograph. The residue image consisting of all the signatures flagged off in previous step are considered here. The residue image is labeled such that each disconnected cluster has a unique label. Grey-scale morphological opening filter is applied on each component in the residue image individually. This reduces the noisy, small concavities along the surface of the clusters giving them a more smooth and circular shape. It also isolate thinly connected signatures.

Step 1: Apply constrained erosion-dilation technique to separate thinly connected particles in the cluster. The foreground of the residual image is eroded one pixel thickness at a time. Ideally, erosion process continues till a unique signature is obtained for each cell nuclei in the region of interest. Any signature size less than size threshold and is not a noisy signature is considered as unique signature of the particle. Such a signature is not subject to further erosion. The signature is tagged with a unique label and number of erosion iterations needed to bring it present size. In the second step, the particle signatures are subject to controlled dilation. The signatures are grown into its neighboring background pixels under certain conditions.

- No two signatures are allowed to overlap or touch one another.
- Signatures are grown only into its immediate neighborhood background voxels.
- The growing process is terminated when the grown region covers all the foreground voxels in original residue image.
- If I_T is the two-tone residue image and I_D is the dilated image with each signature having its own unique label, then $I_{S1} = I_T \wedge I_D$ gives an image where most of the touching particles in the cluster are isolated.

Use relative size filter and the prior information from the training data to extract particles that are isolated by erosion-dilation process. Each individual particle is subject to growing/dilating and controlled grey-scale shrinking to impart them with their original shape.

Step 2: If there are particles still left in the residue image, then a final step of segmentation based on watershed technique is applied [22]. The path generated distance map of the residue image is generated [23]. Homogeneous regions in the distance map are identified and the distance values of those pixels are rescaled to reduce flat fields. This pre-processing of grey scale distance map improves the performance of watershed

techniques in segmentation [24]. Watershed algorithm on a reconstructed grey image can be described in a few steps.

Let *dist(.)* represents the distance value of pixels in the distance map.

Step 1: All the connected group of pixels having maximum distance in the image domain are considered as markers. It may be a single pixel or a group of connected pixels or several groups of connected pixels. The markers are labelled and stored in as a marker image. Let $d_{\max}$ be the maximum distance in the image domain, d_{next} is the next maximum distance level and $d_{\min}$ is the minimum distance value.

Step 2: Pixels having a distance value (d_{next}) and located in the neighbourhood of the labelled regional markers are merged with their neighbouring regional marker.

The isolated pixel or group of connected pixels with distance d_{next} and not having a labelled regional marker in their immediate neighbourhood are considered as new markers and given a new unique label.

Step 3: $d_{\max} = d_{next}$

Step 4: d_{next} = next maximum distance value in the image

Step 5: If the $d_{\max} \neq d_{\min}$ then steps 2, 3 and 4 are repeated.

The resulting image is filtered using relative size filters and the prior information about individual particle features from the training data.

7. Region Growing and Shrinking

Due to extensive preprocessing, particle projections isolated/extracted need not show matching shape properties of its actual projections in the micrograph. It is very important that we acquire actual shape and proper contour of the projections to recognize actual particle and to infer orientation information. For this purpose we consider the isolated objects extracted as just the signatures of the particles. Signatures are grown / dilated to occupy its immediate neighborhood pixels. Number of iterations of region growing defines the neighborhood region the signatures are grown into. Some signature may merge during region growing process. It is also possible that some fragmented particle signatures merge into one real signature. Such a dilated signature is then subject to grey scale shrinking.

Grey scale shrinking is described as follows. The signature is shrunk along its surface only if the surface/boundary pixels have a grey level below a predefined threshold. Low grey scale spots entirely within the objects are not affected. And the object shrinks into its shape defined by grey scale variation in its surface/boundary. All the pixels which are below certain threshold in its grey level are converted into background under the condition that it doesn't create a hole within the object signature.

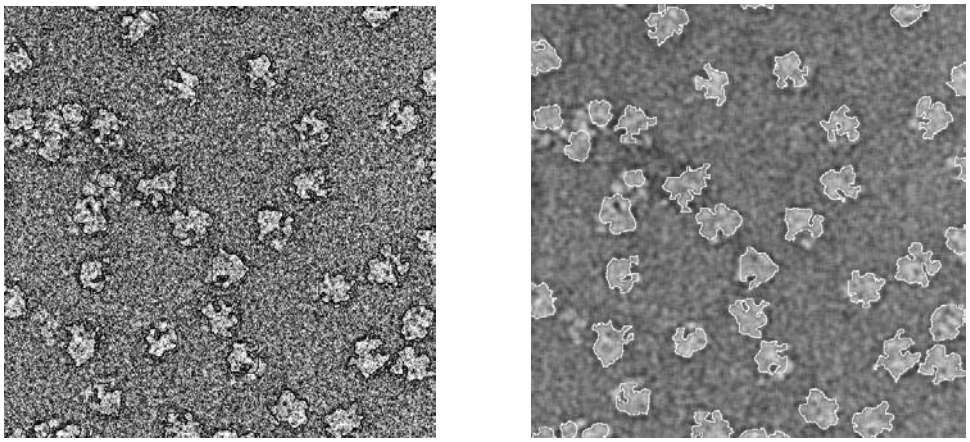

(a) (b)

Figure 8: Result of segmentation shown by superposing boundary of the particle projections on (a) original image (b) on smoothed image

Each individual particle is subject to growing/dilating and controlled grey-scale shrinking to impart them with their original shape. Figure 7(c) and Figure 7(d) and Figure 8, shows the result of segmentation and extraction of single particle projections. Figure 9, shows the result on a complete image (sub-sampled to fit page size).

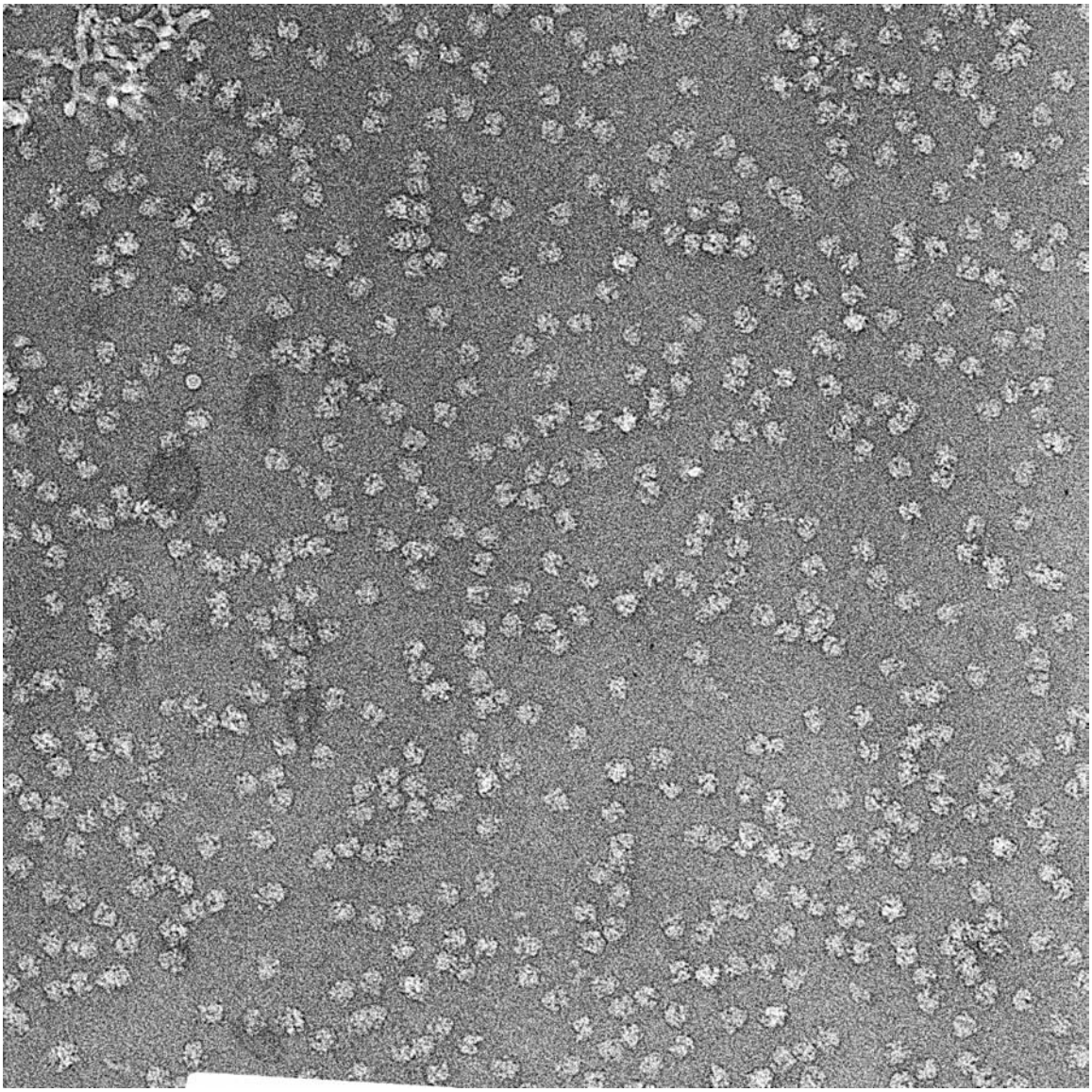

Figure 9(a): Original micrograph (sub-sampled to fit in a page)

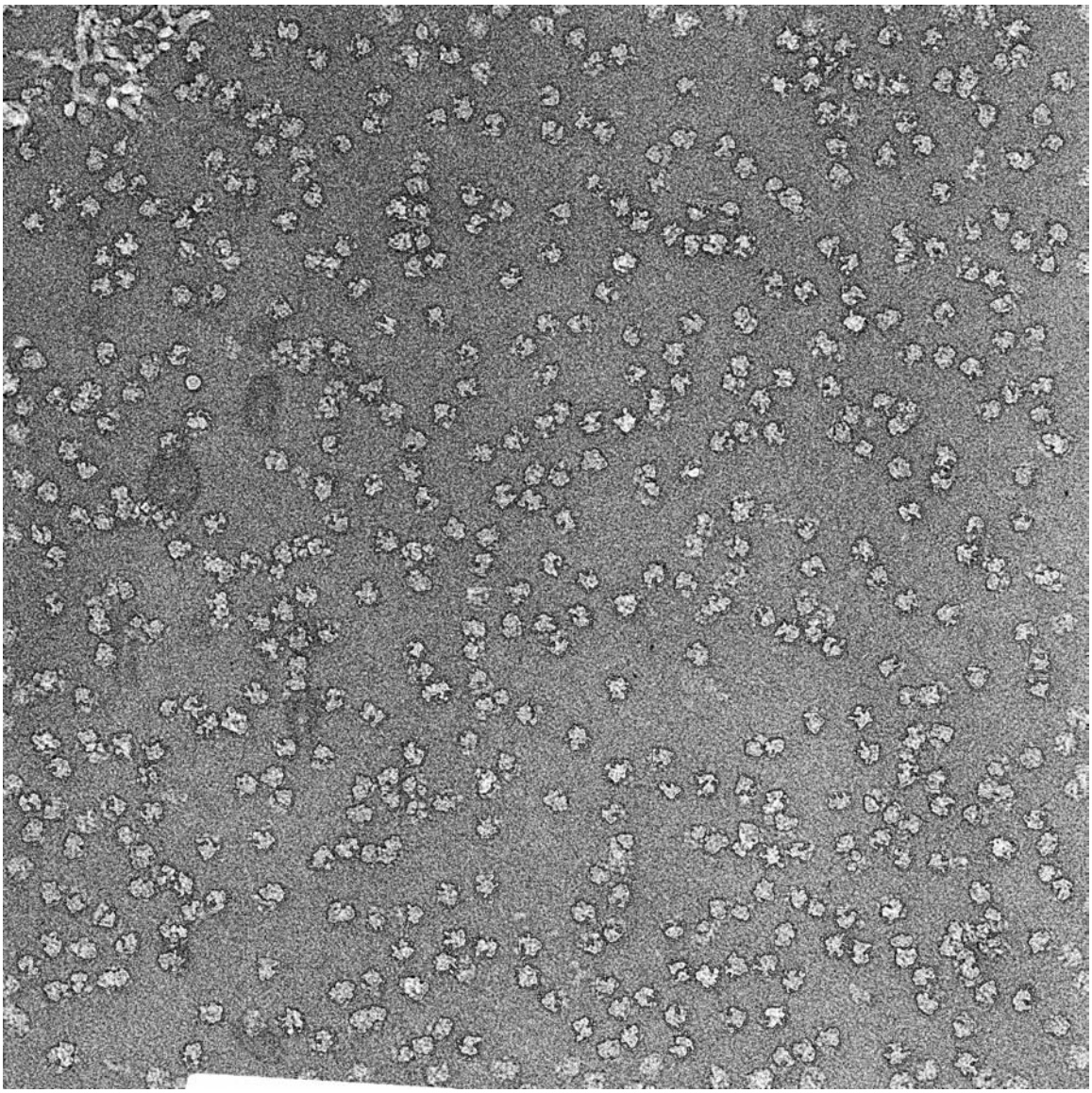

Figure 9(b): Boundary of the particles are superposed on original micrograph (sub-sampled to fit the page)

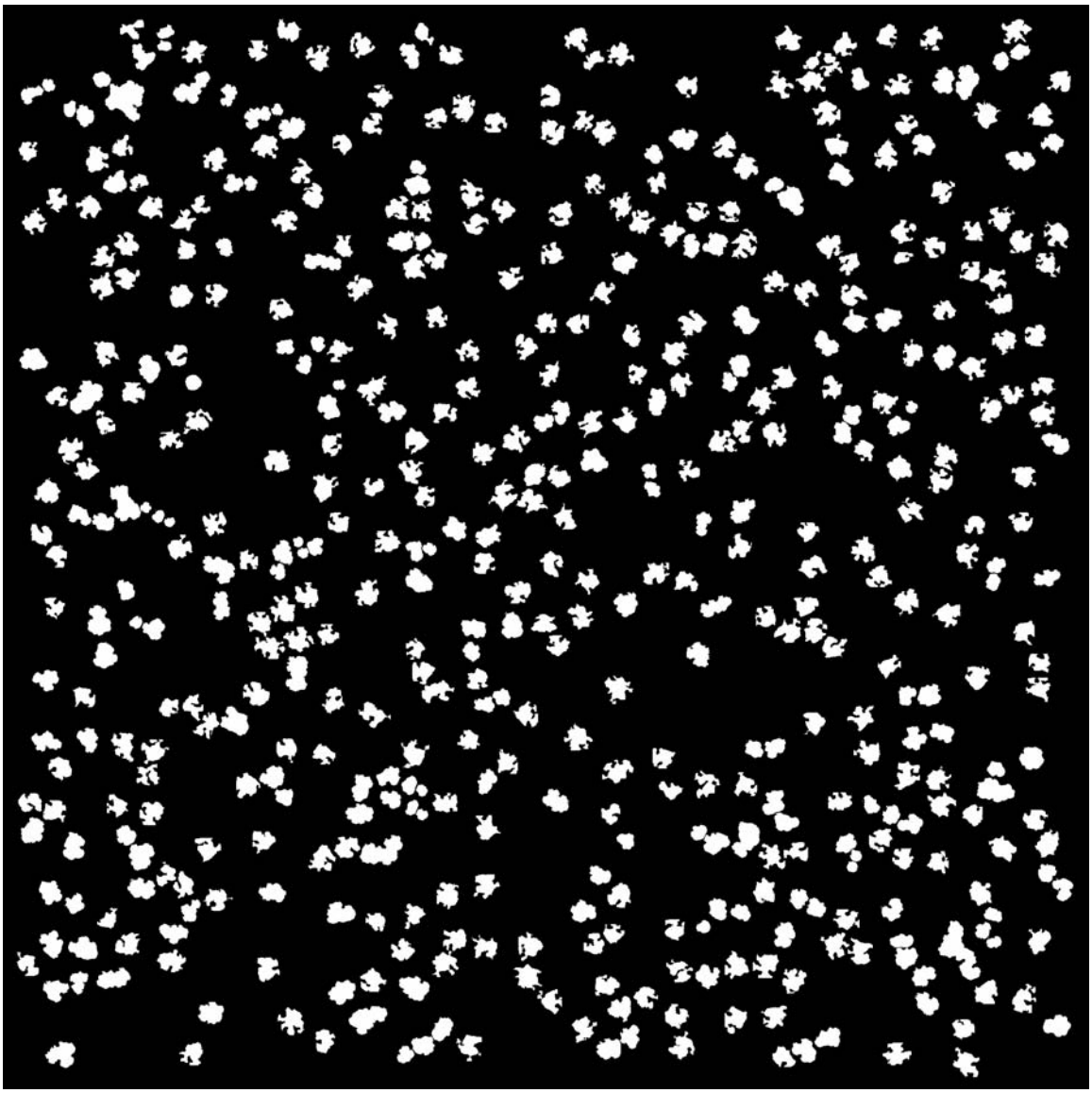

Figure 9(c): Two tone version of the segmented and isolated particle signatures (sub-sampled to fit the page size).

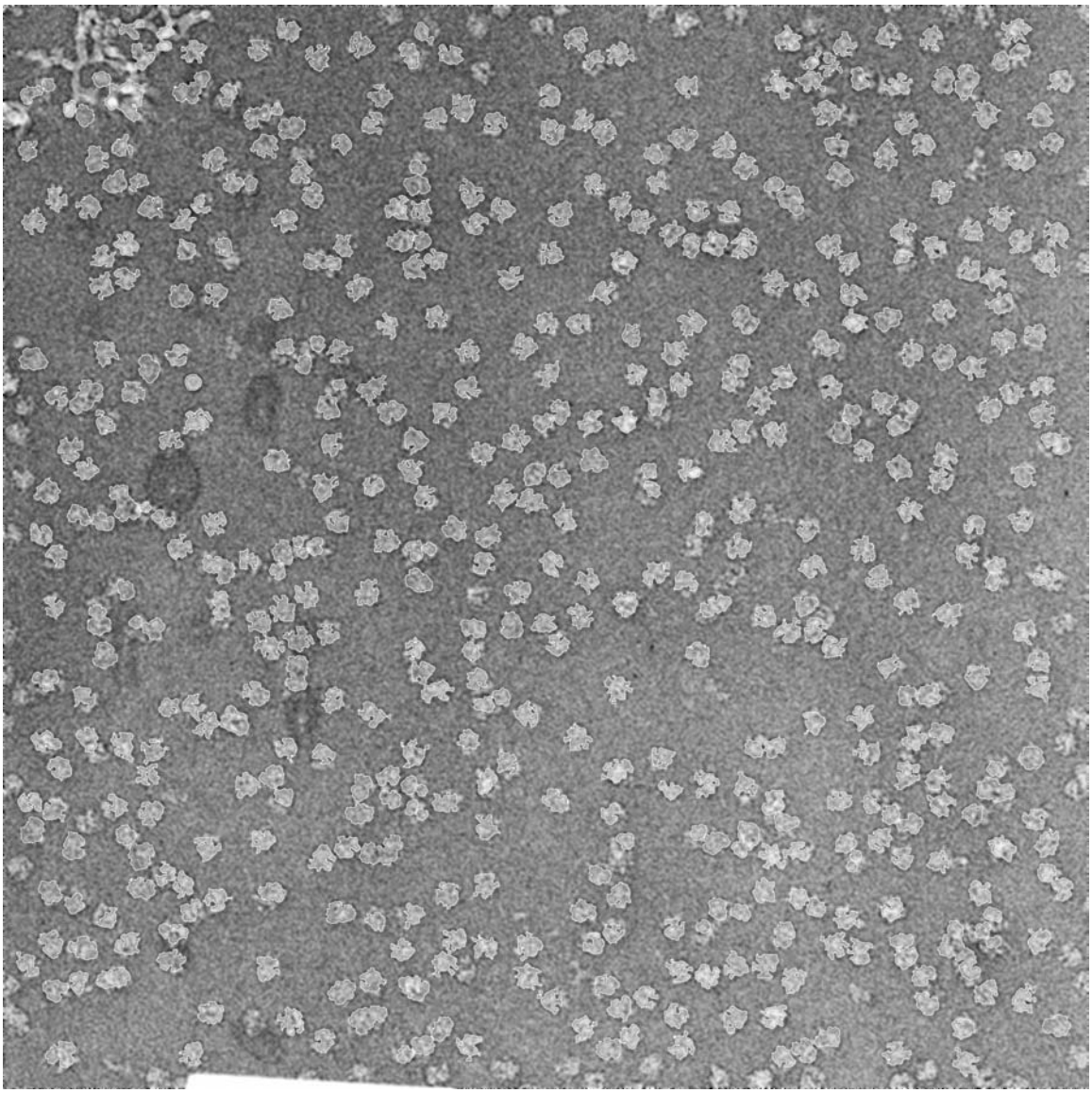

Figure 9(d): Segmented particle boundary superposed on smoothed original image (smoothed by 7x7 average filter and sub-sampled to fit in a page).

8. Second Stage of Analysis

From the results shown in Figure 9, it is possible that in the first stage of particle extraction, one can miss a few or several particle projections or in some cases a cluster of particle projections due to improper parameter settings or due to some poor image acquisition set up (see a brightness saturated strip at the bottom of Figure 9(a) that cannot be explained in the contests of micrograph of particles). Thus, a second stage of analysis is necessary to identify missed particle projections and extract them from the images.

Second stage of analysis has following steps.

1. Replace every segmented particle projection in the original unprocessed micrograph by a background texture.
2. Smooth the resulting image with a Gaussian kernel having high standard deviation (has to be set experimentally or by using training data sets)
3. Open the image with grey scale morphological filter
4. Threshold the image at an appropriate value.
5. Component label the foreground objects
6. Calculate average size of the objects by lower $\alpha-$cut filter. In lower α-cut filter, first 'N' number of objects in the ordered set of objects (ordered based on size) are not considered for calculating average value.
7. Find relative size of each object and filter-out all those objects whose relative size is less than 0.75 (set experimentally). This value has to be set on the basis of training sets in one complete experiment.
8. Segment the foreground image by morphological opening. Extract those objects whose features confer with particle projections extracted in the first stage.
9. If necessary, apply erosion-dilation segmentation process and extract all the individual particle projections in the residue image.

Residue image is then discarded as noise.

9. Construction of sub-images of each particle

Our aim is to extract each particle projection as a small sub-image. All the sub-images should have the same size (same number of columns and rows) so that they can be compared and/or averaged for further analysis towards 3-D shape construction.

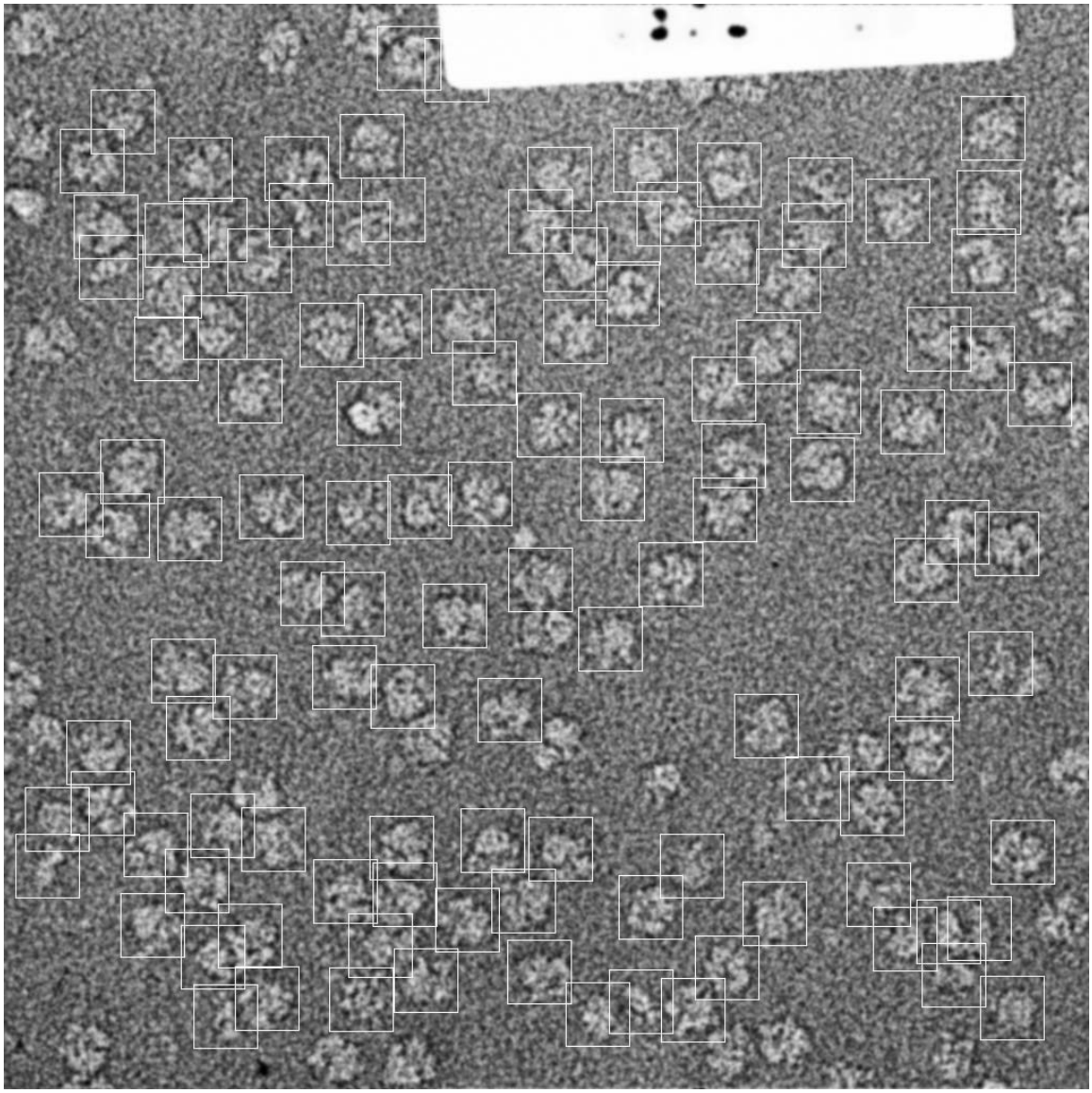

Figure 11: Result of recognizing and boxing the particles. Shown on a different data set.

1. Find the centroid of each particle projection signature that is segmented from micrograph.
2. Find the longest distance between centroid and the particle projection boundary in each segmented particle.
3. Find the maximum distance d_{max} among all particle projections in the micrograph.
4. Extract a sub-image of the size d_{max} x d_{max} around each segmented particle projection such that centroid of the sub-image and centroid of the segmented particle coincide

5. If a particle signature from neighboring particle appears, then replace those pixels of noisy signature by the similar texture pattern that surrounds the rest of the particle.

Resulting sub-images represent single particle projections and each image has the same size. This allows the recognition of those projections with the same orientation and hence averaging of such projections to reduce noise and build 3-D view. Figure 11 and Figure 12, shows the result of boxing segmented particle projections.

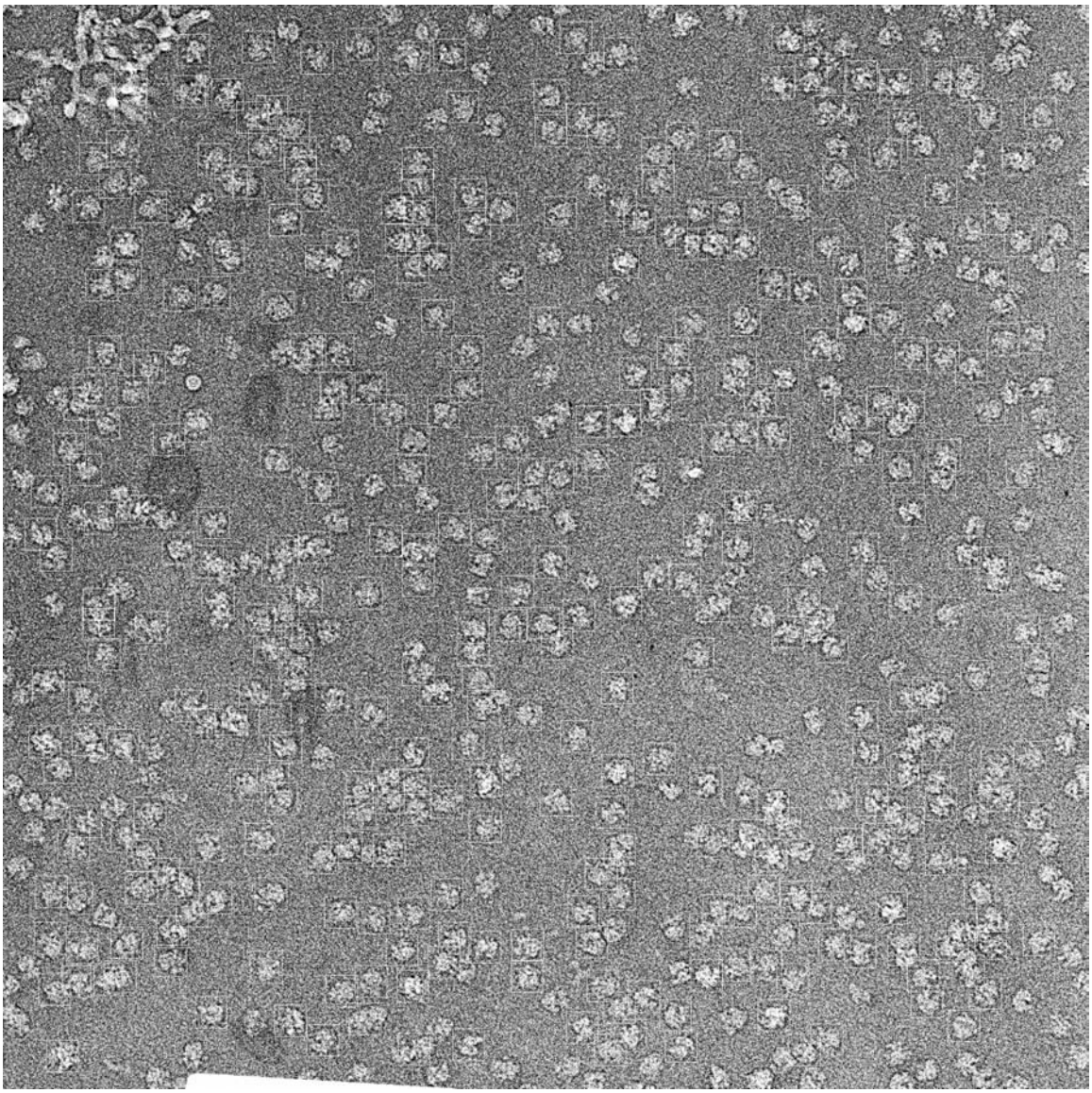

Figure 12: Result of boxing particles on a larger data set used through-out the report

III. Experimental Results and Discussion:

Basic idea behind the methodology is to stretch the difference between background and particles as well as separate segmentation and shape-extraction

procedures. Pre-process the image to an extent that the standard segmentation algorithms can successfully execute and then process each segmented particle image to reconstruct its actual shape. After contrast enhancement and background cleaning, objects are forced have circular shape by morphological filtering with circular structuring elements. Single particle signatures are separated by relative feature filters. Clusters that are more-or-less convex showing concavity where the particles are located very close to one another (or touching one another) are processed by erosion-dilation and watershed techniques. Single particles signatures are again isolated by relative feature filtering. Actual shape of the particle is extracted by considering each signature individually and processing a small box image around the signature.

Figure 13, shows the graphical user interface built for analysis of micrographs and extraction of particle projection signatures. On a 2048x2048 image with about six hundred particle images, the program took ten minutes for multi-stage segmentation and boundary extraction. The program is implemented in Interactive Data Language (www.rsi.com). Efficiency of the program is directly related to quality of the image and the number of single isolated particles present as well as number of particle clusters present. More the number of clusters, slower the program is. This is because, each cluster is handled individually for segmentation purpose and reconstructing its original shape.

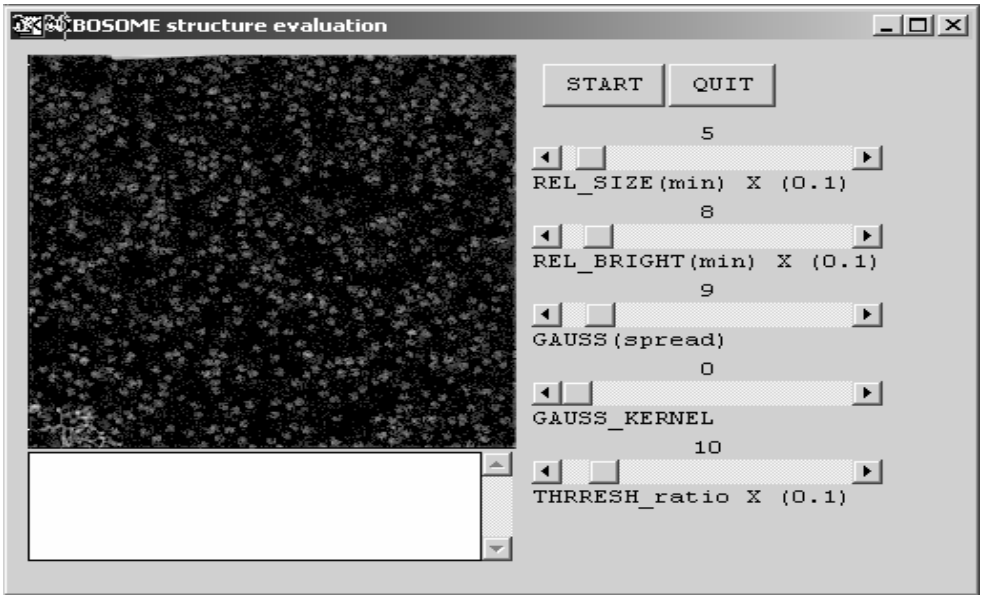

Figure 13: Graphical User Interface for extraction of macro-molecule signature from the cryo-micrograph.

Software works on the basis of some pre-set parameters such as structuring element size for morphological filtering, tuning constant for thresholding, kernel size and standard deviation for Gaussian smoothing, etc. These parameters can be made adaptive after working on a large set of images with various image acquisition set ups. We are in a process of acquiring more data sets to improve the robustness of the software and make it as general purpose as possible.

Stretching the difference between background and particle images is observed to be most effective method to extract particles for boxing purpose. It has been discussed that the method of obtaining a macromolecule structure by subtracting an image of the same area, one with and one without molecule has become obsolete after image averaging technique has facilitated separation of single molecule projections from their background [17]. Our opinion is that "image difference method" works on the assumption that the two images, one with and one without molecule, are essentially same in its image features except for the absence of molecule projections in one image. This assumption might not be correct when we are working with electron micrographs. It is almost impossible to use the same specimen to collect both the images as the imaging technique is destructive of the specimen. Assumption that the two specimen-beds (thin ice) have same image characteristics is highly debatable. The noise pattern produced by the same source at two different times need not be same. In such a situation, instead of taking two images one with molecule and one without molecule, it is better to collect large number of images without molecule under varying imaging conditions and construct a global/general background pattern. It can be argued that larger the number of data sets used for constructing this background pattern, more closer it is to real background variation in the data sets. Filters designed to suppress structural noise based on this general background-image model might have better chance in reducing the noise without doing much harm to molecule projections in the image. We are in a process of collecting micrographs of ice of varying thickness and without macro-molecules, under different imaging protocols to construct a background model and test the hypothesis on "image difference" method.

Another important area where we would like to concentrate is to use edge preserving smoothing techniques in the pre-processing stages. Techniques based on

partial differential equations [25], asymmetric Gaussian kernels, etc. will be tested and evaluated for its effectiveness in stretching the difference between particle images and its background. We would also like to explore Fourier space for reducing noise in the image and stretching the contrast between particle images and common background.

A training data set for each set of experiments will be built and the identification of isolated particle images will be made on the parameters set calculated from this training data. If necessary, training data can then be updated with newly recognized particle features. Some of the parameters that are being set externally will be made adaptive based on the features of particle data in the training set.

We would like to evaluate Level Set approach to find the contours of particles in the micrograph [26]. After approximate contouring by simple gradient based methods, closely located and clustered particles are separated from each other using mathematical morphology methods. Then a fixed area around each particle is considered for application of level set approach to find the possible contours of the particles.

Improved graphical user interface with touch button operations for selecting the objects or selecting the processing tools is necessary for biological applications of the software. We plan to redesign the user interface so that micrographs can be viewed in its entirety as much as possible without undertaking too much scrolling of the display window.

Acknowledgement: Authors are very thankful to Wadsworth Center, Albany, New York for providing the data. Dr. Umesh Adiga would like to thank Dr. Joachim Frank, Dr. Huilin Li and Prof. Ken Downing for their constructive comments on the work.

References and recommended reading

1. Henderson R: The potential and limitations of neutrons, electrons and X-rays for atomic resolution microscopy of unstained biological molecules. Q Rev Biophys 1995, 28:171-193.
2. Stowell MH, Miyazawa A, Unwin N: Macromolecular structure determination by electron microscopy: new advances and recent results. Curr Opin Struct Biol 1998, 8:595-600.
3. Chiu W, McGough A, Sherman MB, Schmid MF: High-resolution electron cryomicroscopy of macromolecular assemblies. Trends Cell Biol 1999, 9:154-159.
4. Crowther RA, Henderson R, Smith JM: MRC image processing programs. J Struct Biol 1996, 116:9-16.
5. Beroukhim R, Unwin N: Distortion correction of tubular crystals: improvements in the acetylcholine receptor structure. Ultramicroscopy 1997, 70:57-81.
6. Grigorieff N: Three-dimensional structure of bovine NADH:ubiquinone oxidoreductase (complex I) at 22 Å in ice. J Mol Biol 1998, 277:1033-1046.
7. Yeager M, Unger VM, Mitra AK: Three-dimensional structure of membrane proteins determined by two-dimensional crystallization, electron cryomicroscopy, and image analysis, Methods Enzymol 1999, 294:135-180.
8. Henderson R, Baldwin JM, Ceska TA, Zemlin F, Beckmann E, Downing KH: Model for the structure of bacteriorhodopsin based on high-resolution electron cryo-microscopy. J Mol Biol 1990, 213:899-929.
9. Nogales E, Whittaker M, Milligan RA, Downing KH: High-resolution model of the microtubule. Cell 1999, 96:79-88.
10. Mancini EJ, de Haas F, Fuller SD: High-resolution icosahedral reconstruction: fulfilling the promise of cryo-electron microscopy, Structure 1997, 5:741-750.

11. van Heel M. Unveiling ribosomal structures: the final phases. Curr Opin Struct Biol. 2000 Apr;10(2):259-64.
12. van Heel M, Gowen B, Matadeen R, Orlova EV, Finn R, Pape T, Cohen D, Stark H, Schmidt R, Schatz M, Patwardhan A, Single-particle electron cryo-microscopy: towards atomic resolution. Q Rev Biophys. 2000 Nov;33(4):307-69.
13. van Heel, M., Harauz, G., Orlova, E.V., Schmidt, R. and Schatz, M. (1996) A new generation of the IMAGIC image processing system. Journal of Structural Biology v.116, pp.17-24.
14. van Heel, M. Detection of objects in quantum noise limited images. Ultramicroscopy, Vol. 8, pp. 331-342, 1982.
15. Lutsch G., Pleissner K P., Wangermann G., and Noll F., Studies on the structure of animal ribosomes. VIII. Application of digital image processing method to the enhancement of electron micrographs of small ribosomal subunits. Acta Biol. Med. Germ. Vol. 36, K59, 1977.
16. Frank J., Wagenknecht T., Automatic selection of molecular images from electron micrographs. Ultramicroscopy, Vol. 12, pp. 169-176, 1984.
17. Frank J., Three-dimensional Electron Microscopy of Macro-molecular Assemblies, Academic Press, San Diego, 1996.
18. Andrews D W., Yu AHC., Ottensmeyer FP., Automatic selection of molecular images from dark field electron micrographs. Ultramicroscopy, Vol. 19, pp 1-14, 1986.
19. Harauz G. and Fong Lochocsky A., Automatic selection of macromolecules from electron micrographs by component labeling and symbolic processing. Ultramicroscopy, Vol. 31, pp 333-344, 1989.
20. Lata KR., Penczek P., Frank J., Automatic particle picking from electron micrographs. In: Proceedings of the 52nd annual meeting MSA (New Orleans), (GW bailey, AJ Garret-Reed Eds.), pp. 122-123, San Francisco Press, san Francisco.
21. Nicholson WV and Glaeser RM, Review: Automatic Particle Detection in Electron Microscopy, Journal of Structural Biology, Vol. 133, pp. 90-101, 2001.

22. Umesh Adiga PS, Chaudhuri BB., "An efficient method based on watershed and rule based merging for segmentation of 3-D histo-pathological images", Int. J. Pattern Recognition, Vol. 34/7, pp-1449-1458, 2001.
23. G. Borgefors G., On digital distance transforms in three dimensions, Computer Vision Graphics and Image Processing, Vol. 64, pp. 368-376, 1996.
24. Andre Bleu, Joshua LL. "Watershed based Segmentation and Region Merging", Computer Vision and Image Understanding, Vol. 77, pp. 317-370, 2000.
25. Malladi R., and Ravve I., "Fast difference schemes for edge enhancing Beltrami flow", In: Computer Vision ECCV 2002, Part I, LNCS 2350 (Heyden et al. Eds.), pp. 343-357, 2002.
26. Malladi R. and Sethian JA, "Image processing via level set curvature flow", Proc. Natl. Acad. of Scie., Vol. 92 , pp. 7046-7050, July 1995.
27. Glaeser RM, and Downing KH., "Assesment of resolution in biological electron microscopy", Ultramicroscopy, Vol. 47, pp. 256-265, 1992.
28. Glaeser RM., Kuo I., and Budinger TF., Method for processing of periodic images at reduced levels of electron radiation. In: Proceedings of the 29th annual meeting EMSA, pp. 466-467, 1971.
29. Van Heel M., Schatz M. and Orlova E.V. (1992) *Correlation functions revisited* Ultramicroscopy 46: 307-316.
30. Van Heel M., Winkler H., Orlova E.V. and Schatz M. (1992) Structure analysis of ice-embedded single particles, Scan. Micros. Suppl. 6: 23-42.
31. Van Heel M., Harauz G., Orlova E.V., Schmidt R. and Schatz M. (1996) A new generation of the IMAGIC image processing system, J. Struct. Biol. 116: 17-24.
32. Schatz M., Orlova E.V., Dube P., Stark H., Zemlin F. and van Heel M. (1997) Angular reconstitution in three-dimensional electron microscopy. Practical and technical aspects, Scan. Micros. 11: 179-193.
33. Van Heel M., Orlova E.V., Harauz G., Stark H., Dube P., Zemlin F. and Schatz M. (1997) Angular reconstitution in three-dimensional electron microscopy. Historical and theoretical aspects, Scan. Micros. 11: 195-210.
34. Van Heel M., Goven B., Matadeen R., E.V. Orlova, Finn R., Pape T., Cohen D., Stark H., Schmidt R., Schatz M. and Patwardhan A. (2000) Single-particle

electron cryo-microscopy: towards atomic resolution, Q. Rev. Biophys. 33: 307-369.

35. Stark H., Müller F., Orlova E.V., Schatz M., Dube P., Erdemir T., Zemlin F., Brimacombe R. and van Heel M. (1995) *The 70S escherichia coli ribosome at 23 Å resolution: fitting the ribosomal RNS*, Structure 3: 815-821.
36. Stark H., Orlova E.V., Rinke-Appel J., Jünke N., Müller F., Rodnina M.V., Wintermeyer W., Brimacombe R. and van Heel M. (1997) *Arrangement of tRNAs in pre- and posttranslational ribosomes revealed by electron cryomicroscopy*, Cell 88: 19-28.
37. Stark H., Rodnina M.V., Rinke-Appel J., Brimacombe R., Wintermeyer W. and van Heel M. (1997) *Arrangement of tRNAs in pre- and posttranslational ribosomes revealed by electron cryomicroscopy*, Nature 389: 403-406.
38. Stark H., Rodnina M.V., Wieden H.-J., van Heel M. and Wintermeyer W. (2000) *Large-scale movement of elongation factor G and extensive conformational change of the ribosome during translocation*, Cell 100: 301-309.
39. Harms J., Tocilj A., Levin I., Agmon I., Stark H., Kölln I., van Heel M., Cuff M., Schlünzen F., Bashan A., Franceschi F. and Yonath A. (1999) *Elucidating the medium-resolution structure of ribosomal particles: an interplay between electron cryo-microscopy and X-ray crystallography*, Structure 7: 931-941.
40. Dube P., Wieske M., Stark H., Schatz M., Stahl J., Zemlin F., Lutsch G. and van Heel M. (1998) *The 80S rat liver ribosome at 25 Å resolution by electron cryomicroscopy and angular reconstitution*, Structure 6: 389-399.
41. Dube P., Bacher G., Stark H., Müller Florian, Zemlin F., van Heel M., and Brimacombe R. (1998) *Correlation of the expansion segments in mammalian rRNA with the fine structure of the 80S ribosome; a cryoelectron microscopic reconstruction of the rabbit reticulocyte ribosome at 21 Å resolution*, JMB 279: 403-421.
42. Stewart P., Chiu C.Y., Huang S., Muir T., Zhao Y., Chait B., Mathias P. and Nemerow G.R. (1997) *Cryo-EM visualization of an exposed RGD epitope on adenovirus that escapes antibody neutralization*, EMBO J. 16: 1189-1198.
43. Al Bovik Eds. Image and Video Processing, Academic Press NewYork, 2001.

44. JC Russ, handbook of Biological Image Processing, CRC Press, New York, 1994
45. Goutsias J, Vincent L, Bloomberg D, Eds. Mathematica Morphology and its applications to Image and Signal processing, KAP Press, Boston, 2000
46. Theodoridis S., Koutroumbas K., Pattern Recognition, Academic Press, London, 1999.